

Designable Luminescence with Quantum Dot–Silver Plasmon Coupler

Lian Hu, Huizhen Wu,* Bingpo Zhang, Lingxiao Du, Tianning Xu, Yongyue Chen, and Yong Zhang

We explore a strongly interacting QDs/Ag plasmonic coupling structure that enables multiple approaches to manipulate light emission from QDs. Group II–VI semiconductor QDs with unique surface states (SSs) impressively modify the plasmonic character of the contiguous Ag nanostructures whereby the localized plasmons (LPs) in the Ag nanostructures can effectively extract the non-radiative SSs of the QDs to radiatively emit via SS–LP resonance. The SS–LP coupling is demonstrated to be readily tunable through surface-state engineering both during QD synthesis and in the post-synthesis stage. The combination of surface-state engineering and band-tailoring engineering allows us to precisely control the luminescence color of the QDs and enables the realization of white-light emission with single-size QDs. Being a versatile metal, the Ag in our optical device functions in multiple ways: as a support for the LPs, for optical reflection, and for electrical conduction. Two application examples of the QDs/Ag plasmon coupler for optical devices are given, an Ag microcavity + plasmon-coupling structure and a new QD light-emitting diode. The new QDs/Ag plasmon coupler opens exciting possibilities in developing novel light sources and biomarker detectors.

1. Introduction

Colloidal semiconductor quantum dots (QDs) are promising light-emitting materials because of their unique characteristics, such as their large quantum-size effect, high

quantum yield, wide spectral adjustability, and low synthesis cost. Size-tunable properties through changing the QD size and the composition in the synthesis stages are a hallmark of group II–VI QDs that have been intensively studied.^[1–6] Recent advances in the study of energy transfer between the quantum states and surface states (SSs) of group II–VI QDs have led to the development of a new field.^[7–11] As colloidal QDs mostly are very small (ca. 1–10 nm), the resulting high surface/volume ratio renders a high density of surface states that are generally regarded as non-radiative trap states and, thus, the cause of low quantum yields (QYs) of the QD emitters. The surface trap states of QDs have often purposely been suppressed.^[12] A key issue arises here, namely, can we convert the non-radiative trap states to radiative ones? Recently, the surface trap states of CdSe QDs have been effectively converted to radiative ones by plasmon-resonance methods and the QY of these QDs was greatly enhanced.^[13] Studies have shown that colloidal QDs with rich surface trap states could be used as white-light sources because surface trap states can generate a high-QY broad emission band in the visible region; furthermore, they can be changed by some external parameters.^[14–21]

Dr. L. Hu, Prof. H. Wu, B. Zhang, L. Du, Y. Chen
Department of Physics and State Key Laboratory
of Silicon Materials
Zhejiang University
Zheda road 38, Hangzhou 310027, P.R. China
E-mail: hzwu@zju.edu.cn

Dr. T. Xu
College of Science
Zhejiang University of Technology
Hangzhou, Zhejiang 310024, P.R. China
Prof. Y. Zhang
Department of Electrical & Computer Engineering
Optoelectronics Center
University of North Carolina at Charlotte
Charlotte, North Carolina 28223, USA



DOI: 10.1002/sml.201400094

Surface-state related emission arises from the optical transitions of surface trap states located in the bandgap of QDs, which emerges as a broad peak at the lower photon energy relative to the band-edge emission (BEE).^[12,22] The SS emission (SSE) can be tuned and controlled in both synthesis stages in solution and post synthesis stages in thin solid films.^[14,23,24] The synthesis parameters (e.g., the initial amount and concentration of the reacting materials, temperature, time, etc.) and post-synthesis wet chemical treatments (e.g., ligand modification and medium capping) remarkably influence the properties of SSE. However, post-synthesis wet-chemical treatments usually introduce more defects on the surface of the QDs and form rich-surface trap states, which usually additionally quench the luminescence. Whereas surface states are dominant routes in the non-radiative decay of excited electrons, the resonant coupling of QD emitters-metallic plasmons provides an effective way for extracting the energy of the surface states via radiative decay channels.^[13] This physical approach greatly enhances the intensity of SSE. Though plasmon-enhanced SSE has been reported before,^[25–27] the key factors that may tune the SS–plasmon coupling are yet to be explored.

In this paper, group II–VI QDs with well-defined surface states are synthesized for the tuning of the strong coupling between the QD emitters and plasmons in Ag nanostructures. The adjustability of SS–LP coupling via surface-state engineering, such as surface passivation of QDs during synthesis and surface photoactivation of the QDs after synthesis, is explored. We demonstrate the precise tuning of QD–plasmon coupling through modification of the density of surface states (DOSSs) of the QDs by surface passivation with incorporation of a S precursor, which forms a shell around a CdZnS core during the synthesis procedure. We further show the facile tuning of the QD–plasmon coupling via reducing the DOSSs of the QDs by applying photoactivation (UV-light irradiation) in a post-synthesis stage. An analog to a white-light emitting device using single-size CdZnS QDs is successfully developed by the combination of surface-state engineering and band-tailoring engineering. To illustrate the applications of these QDs/Ag plasmon couplers, we have realized the concurrence of multiple functions in the Ag layer, consisting of plasmon supporting, reflecting mirror, and electrode. An optical microcavity plus SS–plasmon coupling structure is demonstrated in which the SSE of the single-size QDs almost covers the whole visible-light band. The electroluminescence of a newly realized QD light-emitting diode (QDLED) shows bias-sensitive SSEs.

2. Tuning of the SS–LP Coupling via Surface-State Engineering of QDs

Our previous studies have demonstrated the distinct enhancement of the SSE of colloidal CdSe quantum dots (QDs) via coupling to localized plasmons (LPs) in Ag nanostructures.^[13] The strong QD emitter–plasmon coupling makes the emission of a QDs/Ag structure quite different from that of bare QDs. It has been found that an oleic acid (OA) ligand on CdSe QDs plays a critical role in the modification

of an Ag nanostructure by forming a CdSe QDs/Ag coupler, which consequently has an impact on the coupling of the QD emitters with LPs in Ag. However, in the QDs/Ag coupler the modification of SSs on the LP coupling was not studied nor fully understood. Here we take our QDs/Ag couplers and investigate the adjustability of the SS–LP coupling by manipulation of the SSs both during and after synthesis. We call these in-synthesis and post-synthesis tuning approaches to the surface of the QDs the surface-state engineering and the band-tailoring engineering, respectively.

Five batches of CdS QDs with different dot size and a different density of SSs were synthesized. The photoluminescence (PL) spectra and TEM images of the QDs are shown in Figure S1 (Supporting Information). The PL peak positions of the BEEs for the five-batch QDs were at 410, 428, 440, 456, and 472 nm, with a narrow FWHM of 21, 20, 20, 17, and 17 nm, respectively. The estimated dot sizes are 3.1, 3.8, 4.2, 5.1, and 6.0 nm, respectively. The phenomenon of the intense size-dependent enhancement of the SSE was also reproduced in the CdS QDs/Ag couplers. The PL spectra of the CdS QDs/Ag couplers before and after annealing are shown in **Figure 1**. The detailed PL and time-resolved PL decay spectra of the QDs/Si and QDs/Ag are shown in Figure S2 (Supporting Information). It can clearly be seen that the couplers without annealing show more intense enhancements of the SSE for the small-size CdS QDs than the large-size ones whereas the annealing treatment results in more intense enhancements of the SSE for the large-size QDs than the small-size ones. The color bands in Figure 1 indicate a red shift of the SSE. Annealing leads to a red-shift of the dominant LP modes in the QDs/Ag couplers, therefore, the luminescence of CdS QDs with the appropriate size can be changed significantly when the SSE is resonantly coupled with the LP modes in Ag.

As seen in Figure 1, the enhancement of the SSE shows a large difference before and after annealing. This interesting phenomenon can be understood clearly by the following plasmonic interaction picture. In a metal/dielectric system, the plasmonic mode (or frequency) in the metal is primarily determined by the dielectric function of the metal, but the geometry (i.e., grain size and shape) also has an impact. Shown in Figure S5 in the Supporting Information, the as-deposited Ag film consists of small grains with sizes of about 10–30 nm, however, the annealing treatment causes a great change in the Ag morphology by reshaping the small Ag grains into larger ones with irregular shapes. Small Ag particles have a higher plasmonic frequency than large Ag particles.^[28,29] Thus, the annealing process leads to a red-shift of the LP modes in the CdS QDs/Ag couplers. The resonance of the SSEs of CdS QDs with LP modes in the Ag particles causes a strong light-absorption/scattering and intensely enhanced local electromagnetic fields that greatly affect the radiative recombination of the QDs. Therefore, the as-deposited small Ag grains favorably enhance the SSEs of small-size QDs whereas the larger Ag particles formed by annealing favorably enhance the SSEs of large-size QDs.

We found that the luminescence properties of the annealed QDs/Ag couplers are more stable than those of couplers without annealing. This phenomenon can be

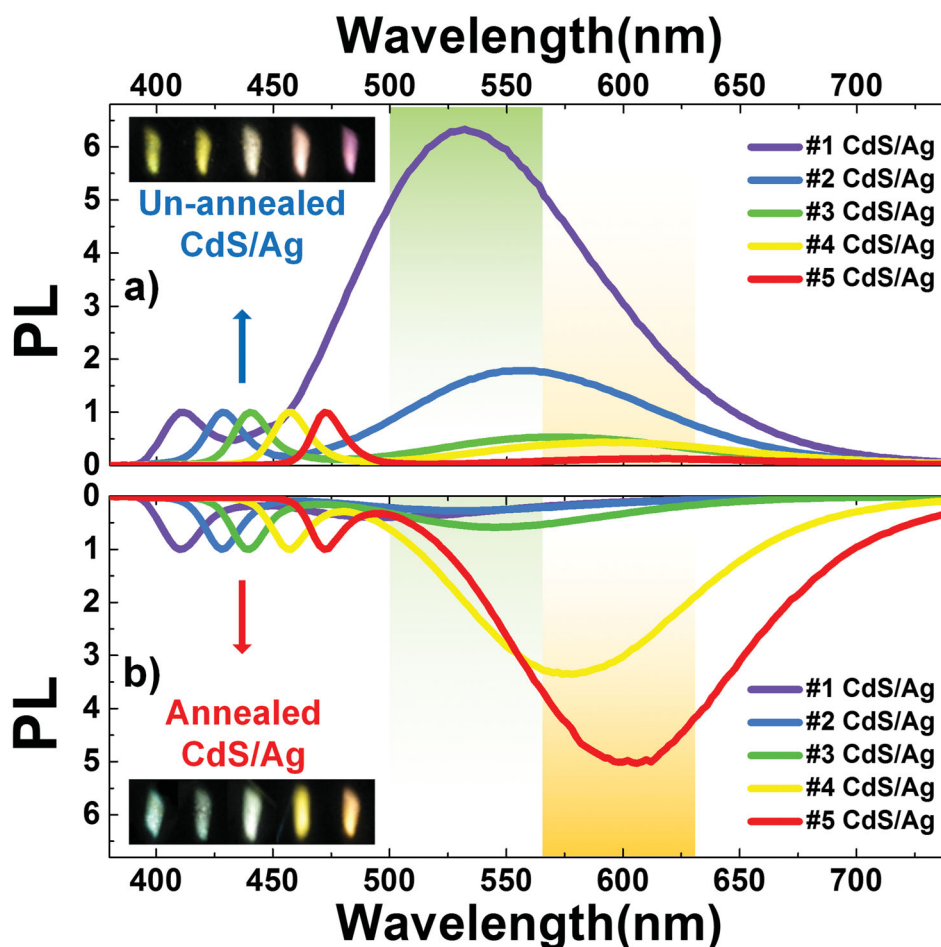


Figure 1. PL spectra of the QDs/Ag/Si samples with and without annealing and the corresponding light spot (Excitation line: 325 nm).

ascribed to the following two factors: First, the surface of the metallic Ag film becomes more stable (lower activity) after annealing in OA (residue in the QDs layer). Second, the OA residue in the QDs, which acts as an etchant to Ag, decreases because of the intensified chemical and physical processes at the annealing temperatures, such as redox reactions, desorption, and evaporation.^[30] A notable reduction of the OA residue in the QDs layer by annealing was observed by FTIR (spectra shown in Figure S4, Supporting Information).

The SS–LP coupling evidently improves the energy transfer from the band-edge excitons to the SS-related excitons. As shown in Figure S2 in the Supporting Information, the plasmon-enhanced SSEs of the CdS QDs/Ag couplers mostly have longer lifetimes than the corresponding SSEs of the CdS QDs/Si couplers. This phenomenon is different from the previously reported plasmon-enhanced BEE lifetimes where the intensity enhancements of the BEEs were often accompanied with a reduction in the decay lifetimes because resonant plasmons in the metal commonly enhance the radiative decay rate (k_r) of the BEEs. The contradictory phenomenon observed in CdS QDs/Ag couplers, namely, the enhanced SSE intensities and increased decay lifetimes, can be explained by the Purcell effect. The LP coupling not only

increases the radiative decay rate (k_r) but also suppresses the non-radiative decay rate (k_{nr}) of the QDs SSEs. The detailed data and analysis are given in Figure S2 (Supporting Information).

The intensity-enhancement factors of the SSEs in the QDs/Ag couplers are dependent on the thickness of the QD layer. A huge enhancement factor as high as 580 (Figure S5, Supporting Information) was realized by optimizing the thickness of the QD layer, exceeding almost all the previously reported enhancement factors of plasmon-enhanced emissions of QDs. We further found that after annealing a thin Ag film with discrete surface morphologies presents primarily similar LP-enhancement characteristics to a thick and continuous-morphology Ag film (Figure S6, Supporting Information). These results indicate that the LP coupling in the QDs/Ag couplers is non-sensitive to the initial morphology and the thickness of Ag. Thus, the proposed fluorescence/metal system for luminescence enhancement does not need any accurate tailoring of the shapes and sizes of the Ag nanostructures nor the coordination of the distance between the QD emitters and the Ag particles as is the case in many previous works.^[31–36] Therefore, our QDs/Ag plasmon couplers for luminescence enhancement are readily realized and cost efficient.

2.1. In-Synthesis Tuning of SS–LP Coupling via Surface Passivation of QDs

Precise manipulation of plasmonic coupling is a key issue to realize new light sources on the nanoscale. Many research efforts have been reported on the tuning of plasmonic coupling via complicated fabrications of metallic nanostructures. On the contrary, we demonstrate here the facile and precise tuning of LP coupling via modification of the SSs of the QDs emitters both during and after synthesis.

SS–LP coupling can be readily manipulated by changing the SSs of the QDs during the synthesis stage. We change the DOSSs of the QDs by surface passivation through incorporation of a S precursor for the formation of a ZnS shell on a CdZnS core during the synthesis process. To strengthen the function of the SSs while maintaining the BEE at the same energy, alloyed CdZnS QDs were synthesized to demonstrate the possibility of tuning the SS–LP coupling. Five batches of alloyed CdZnS QDs were extracted in the synthesis stage: three batches of CdZnS QDs were obtained after 1, 4, and 8 min from the first injection of S precursors; two batches of CdZnS/ZnS QDs were obtained after 2 and 30 min from the second injection of S. **Figure 2a–d** shows the typical TEM images of four different-sized QDs (two batches of CdZnS QDs obtained during the process for core growth and two batches of the CdZnS/ZnS QDs obtained during the stage of the shell formation). The estimated sizes of the four batches were 3, 5, 7, and 10 nm, respectively. Shown in **Figure 2e** are the peak wavelengths of their BEEs, which are 446, 446, 450, 446, and 440 nm, respectively, with a FWHM of around 16 nm. The competition between the increased size of the particles and the decreased Cd/Zn ratio during the reaction limits the BEE peak position variations to a small range so that the SS effect can be studied separately. **Figure 2e** displays that the core–shell structure evidently suppresses SSE but enhances BEE because of the surface passivation by the formation of a shell on the surface of the QDs.^[37–40]

The change of DOSSs of the QDs significantly modifies the SS–LP coupling of the QDs/Ag couplers both with and without annealing (**Figure 2f–o**). The QDs with shorter growth time evidently have higher DOSSs, corresponding to the stronger SS–LP coupling. For example, the SSE of the QDs/Ag dominates the PL in **Figure 2g** whereas the SSE of the QDs/Ag in **Figure 2l–o** is not prominent. Because of the strong SS–LP coupling the luminescence color of the QDs/Ag is in sharp contrast to that of the QDs/Si in **Figure 2g**, but the colors of the QDs/Ag and QDs/Si in **Figure 2o** can hardly be discriminated because of the effective passivation of the SSs. It can be concluded that the surface-state engineering of the QDs during synthesis can profoundly tune the QDs–LP coupling.

2.2. Post-Synthesis Tuning of SS–LP Coupling Via Surface Photoactivation of QDs

It has been demonstrated that the passivation of the SSs by shell formation on the QDs during the synthesis stage

can effectively modify the SS–LP coupling. In this section, we further show the facile tuning of the SS–LP coupling by modifying the SSs of the QDs emitters in a post-synthesis stage. Photoactivation (UV-light irradiation) of the surfaces of synthesized QDs can lower the DOSSs as well, without changing the size of the QDs. A chemical picture of UV-light irradiation on the QDs in ambient air shows that oxidation of the QD surface effectively passivates the SSs. A sample similar to that shown in **Figure S2j** in the Supporting Information (#5 CdS QDs) was irradiated by a 405-nm picosecond laser and the PL spectra were measured at regular time intervals. **Figure 3a,b** shows the PL spectra of the #5 CdS QDs/Ag and #5 CdS QDs/Si at different intervals in the irradiation process. Photoactivation greatly changes the PL spectra of the QDs/Ag couplers. The PL spectra of the QDs/Ag were fitted by three Gaussian peaks (the inset in **Figure 3c**): one for the BEE and two for the SSE. The two fitted SSE peaks correspond to two major SS levels in the bandgap of the QDs. The temporal evolution of the PL intensities versus the irradiation time for the three peaks are shown in **Figure 3c**. This shows that the BEE intensity increases initially and then decreases, whereas the two SSE peaks decrease with prolonging irradiation time. The temporal evolution of the lifetimes of BEE and SSE, plotted in **Figure 3d**, show that there is little change in the BEE lifetime, but the SSE lifetime decreases, similar to the SSE intensity in **Figure 3c**. The fact that the BEE intensity increases in the first 20 min indicates that photoactivation passivates the SSs in this first stage. At this point, the surface of the QDs adsorbs O₂ and forms an oxide surface (such as CdO and SO₄²⁻).^[41–43] The dangling bonds on the surface of the QDs are passivated by the oxidation process, resulting in a decrease of the DOSSs. The reduction of the DOSSs by 405-nm light irradiation may cause the suppression of the possible electron transfer from band-edge states to the SSs, in other words, the energy transfer rate from the band edge to the SSs, k_{ET} in Equation S3 (Supporting Information), decreases. The little variation in BEE lifetime in the irradiation process suggests that the sum of the radiative decay rate (k_r), non-radiative decay rate (k_{nr}), and k_{ET} remains unchanged. From Equations S5 and S6 (Supporting Information) we calculated that k_r increases in the first 20 min, which is in accordance with the enhanced BEE intensity (**Figure 3a,c**). For the SSE, things are different in the first 20 min: because of surface oxidation of the QDs the DOSSs decrease thus k_{nr} decreases, whereas the lifetime of the SSE changes little as shown in **Figure 3d**, indicating that k_r increases at this stage. The reduction of the DOSSs may dominantly influence the SS recombination.

After the first 20 min, the excessive irradiation on the QDs causes some desorption of the Cd and S atoms on the surface of the QDs, therefore, more vacancy defects are introduced on the surface. Consequently, more photo-generated electrons in the QDs could transfer to surface defect states and the BEE begins to quench in a slow rate. During the irradiation time of 40–100 min, both BEE and SSE decrease slowly following a similar trend (**Figure 3c**) whereas the SSE lifetime becomes shorter (**Figure 3d**). The

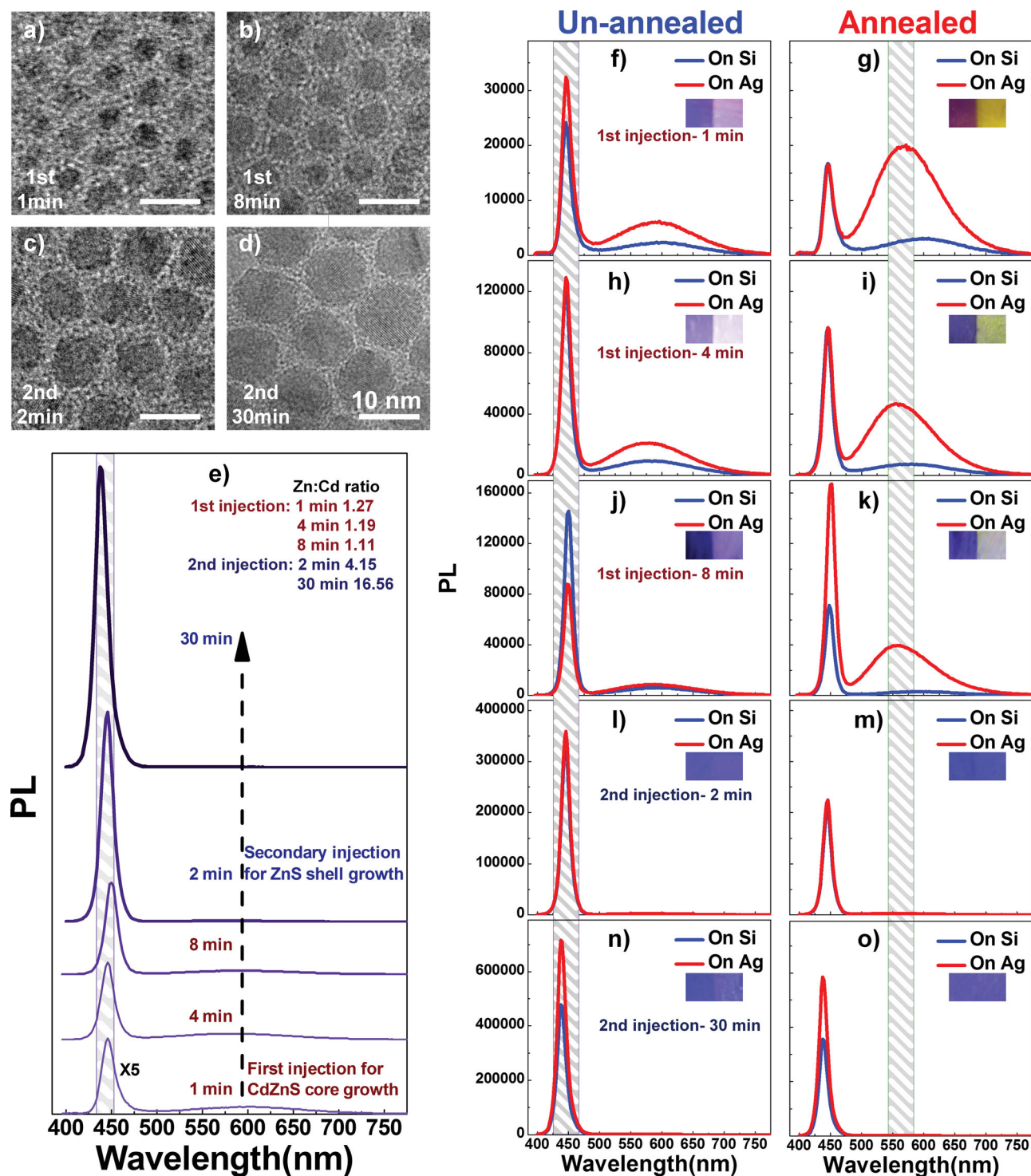


Figure 2. a,b) TEM images of the alloyed CdZnS cores obtained after 1 min (a) and 8 min (b) of the first injection of S precursor. c,d) TEM images of the CdZnS/ZnS QDs obtained after 2 min (c) and 30 min (d) of the second injection of S precursor. e) Temporal evolution of the PL spectra of the alloyed QDs obtained at different growth times in reaction (1, 4, and 8 min after the first S injection for the alloyed core growth and 2 and 30 min after the second S injection for the shell formation). f–k) PL spectra of the 3 batches of CdZnS QDs on Si and on Ag. l–n) PL spectra of the 2 batches of CdZnS/ZnS QDs on Si and on Ag.

increment in surface defects caused by excessive irradiation may differ from the SSs (dangling bonds) of the as-synthesized samples. It can be concluded that moderate photoactivation can further tune the SS–LP coupling to influence the emission of the QDs/Ag couplers by passivation of the

SSs and increase the radiative rate of the BEE. However, the tuning approach of the shell growth on QD cores seems more effective in the suppression of the SSE in comparison to the photoactivation approach for the QDs/Ag plasmon coupler.

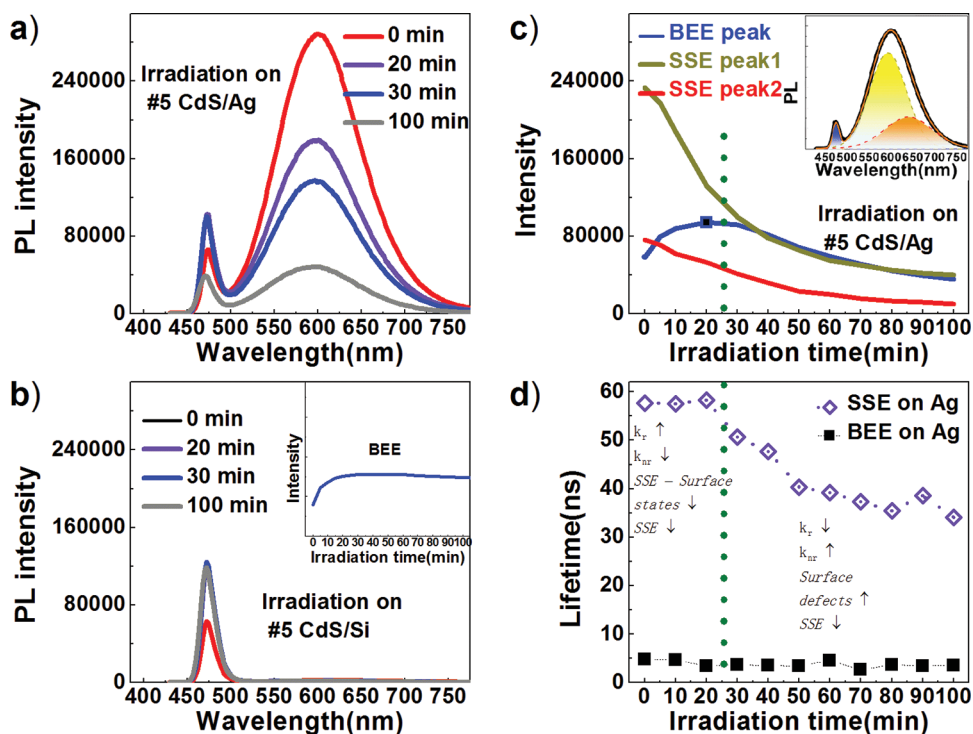


Figure 3. a) PL spectra of #5CdS QDs/Ag with 405 nm irradiation. b) PL spectra of #5CdS QDs/Si with 405 nm irradiation (Inset: temporal evolution of the intensity for the BEE). c) Temporal evolution of the intensities for the fitted peaks (Inset: The PL spectra of the #5 CdS QDs/Ag are fitted by one BEE peak and two SSE peaks). d) Temporal evolution of the lifetimes for the SSE (600 nm) and BEE (472 nm) in the irradiation process.

2.3. Realization of White-Light Sources Using Single-Size QDs by Combining Surface-State Engineering and Band-Tailoring Engineering

In a typical white-light emitting device (WLED), white light is generated via superposition of a narrow blue-light emission from InGaN/GaN LED chips (λ 470 nm) and a broad yellow-light emission (λ 500–700 nm) from YAG:Ce phosphors. We demonstrate here an analog of a WLED using single-size CdZnS QDs that are tuned through surface-state engineering and band-tailoring engineering. In the CdZnS QDs, the PL spectra clearly show a narrow BEE peak and a broad SSE with longer wavelengths. Similar to typical white-light spectra of InGaN/GaN LEDs it is possible to realize white luminescence from single-size QDs as well by tuning the two emission peaks of the QDs to have suitable wavelengths and intensity ratios. Commonly, the wavelengths of the emission peaks of the QDs are fixed from the synthesis stage of the QDs. In our previous work, very small CdSe QDs were synthesized to obtain a blue BEE (at ca. 460 nm) and white luminescence from a CdSe QDs/Ag coupler was demonstrated.^[13] But the small CdSe QDs with the blue BEE peak were not stable as their high surface energy easily caused aggregation of the QDs during annealing. Moreover, in the small CdSe QDs the relatively weak blue BEE peak was generally accompanied by a prominent SSE peak, which made it impossible to achieve WLEDs. Though CdS QDs seem a good alternative white-light source and we have been able to realize approximate white-light emission from our CdS QDs on Ag in this work (Figure 1), the BEE and SSE peaks of the CdS QDs are difficult to tune simultaneously. The band-

tailoring engineering of the alloyed QDs has proven to be a valid way for the precise positioning the BEE peak mainly through adjusting the amount of the initial precursors.^[37–40] This is, however, not sufficient to realize white-light emission from the single-size QDs. It is also critical to tune the SSE of the QDs. By combining the tuning approaches stated above (surface passivation of the QDs in the synthesis stage, SS-LP coupling, and surface photoactivation of the QDs/Ag couplers after synthesis), white-light emission from the single-size QDs can be achieved.

Semi CdZnS/ZnS core-shell QDs structures with a partially passivated core surface were prepared for this. The preparation method of the semi core-shell QDs is similar to that stated in Section 2.1. The difference is that the Zn:Cd ratio (1.5) and the amount of second injected S for the synthesis of the semi CdZnS/ZnS core-shell QDs are smaller than those for the full CdZnS/ZnS core-shell QDs, which causes an incomplete ZnS shell coating that partially passivates the surface dangling bonds on the core surface. An expected result of the semi CdZnS/ZnS core-shell structure was the enhancement of the BEE and the alleviation of the plasmon-enhanced SSE which provides an independent parameter to tune the two emissions.

The schematic illustration of the preparation for the semi CdZnS/ZnS core-shell QDs/Ag couplers is shown in Figure 4a,b. Figure 4c shows the evolution of the PL spectra for the semi CdZnS/ZnS QDs using the surface-state engineering approach. The PL spectra of both QDs/Si and QDs/Ag are plotted for comparison. The annealing treatment of the QDs/Ag coupler leads to the enhancement of the coupling between the QDs and LPs in Ag. The SSE at 596 nm

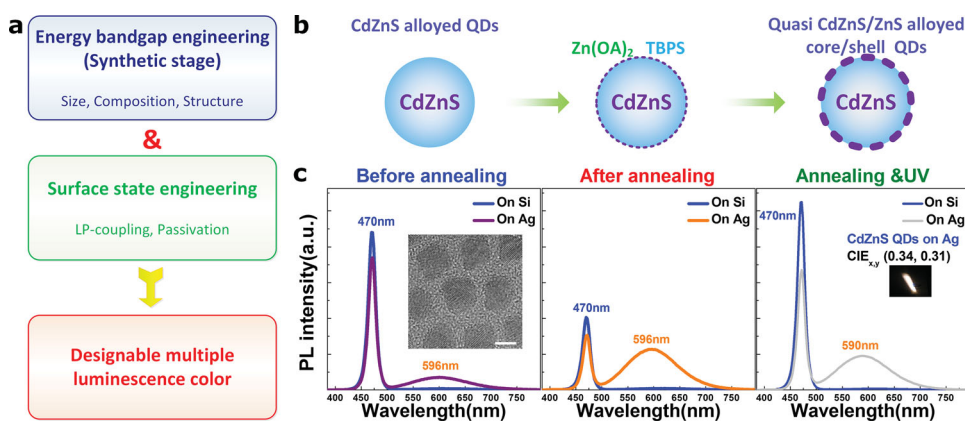


Figure 4. Combination of the band-tailoring engineering and SSE-tuning engineering. a) Schematic illustration of the combination of band-tailoring engineering and SSE-tuning engineering. b) Schematic illustration of the preparation for the semi CdZnS/ZnS core–shell QDs. c) The application of surface-state engineering on the CdZnS/ZnS QDs for white luminescence (Inset: the HRTEM image of the QDs (bar: 5 nm) and a photograph of the light spot excited by the 325-nm line of a Xe lamp).

is clearly enhanced whereas the BEE at 470 is suppressed. The luminescence color of the annealed QDs/Ag coupler is yellow because of the blend of the blue BEE and the orange SSE. After UV-light irradiation on the sample, the BEE intensity increases notably whereas the SSE of the QDs/Ag declines slightly. As a result, a white-light source is realized by the superposition of the two emissions from the single-size QDs on Ag. The 1931 CIE coordinates for the realized white-light source are (0.34, 0.31).

3. Optical Devices with Enhanced SSE

In the QDs/Ag plasmon couplers stated above the layer of QDs acts as both an intense luminescence emitter and a modifier of the plasmonic properties of the Ag nanostructure. Our goal was to further exploit the versatility of the Ag metal. Being a noble metal Ag has multiple functions, such as acting as a plasmon carrier, optical mirror, or electrode, etc. Optical devices with unique functions could be formed by utilizing the QDs/Ag coupler. Here we propose two application examples of the QDs/Ag coupler in optoelectronic devices: 1) An optical microcavity with a simple structure of Ag/PMMA-QDs/Ag (PMMA: polymethylmethacrylate) in which the Ag films not only act as the carriers of the LPs for the SSE enhancement of the QDs, but also serve as the cavity mirrors with high optical reflectivity; 2) A QD light-emitting device (QLED) in which Ag acts as both the electrode and the optical confinement layer for electroluminescence.

3.1. Optical Microcavity-modulated + Plasmon-Enhanced SSE

In an optical microcavity structure, the typical thickness of an active layer is designed to be $\lambda_0/2n$ where λ_0 is the wavelength of the emission peak and n is the refractive index of the active layer. The SSE peak of the QDs is very broad and can be strongly enhanced (thus higher gain) by forming a QDs/Ag coupler. When the broad and plasmon-enhanced SSE peak is taken as the gain spectrum of the active layer,

the important advantage is that λ_0 could be tuned over a wide range. In this designed microcavity structure, both the PMMA-QDs and the Ag layers serve multiple functions, as the active layer and the SP modifier, and the LP carriers and the mirrors, respectively.

The preparation of the plasmon-enhanced Ag/PMMA-QDs/Ag microcavity structure is shown in **Figure 5a**. A thick Ag film (ca. 250 nm) with high reflectivity was firstly deposited on a Si chip. Then the blend of PMMA – CdS QDs ($\lambda_{\text{BEE}} = 456$ nm) dissolved in toluene was spin-coated on the Ag film to form an active layer (ca. 200 nm) and followed by annealing to enhance the SSE. A top Ag layer (ca. 50 nm) was finally deposited on the PMMA-QDs layer. An SEM image of the cross section of the microcavity is shown in **Figure 5b**. The PL and reflection spectra of the microcavity structure with the cavity mode at 624 nm are shown in **Figure 5c**. The dotted line in **Figure 5d** shows the PL spectrum of the annealed PMMA-CdS QDs/Ag which is the recurrence of the plasmon-enhanced PL spectrum shown in **Figure 1**. PL spectra of microcavities with active layers of different thicknesses and excited by a 405-nm laser are shown in **Figure 5d**. When the microcavities are excited by the 405-nm laser, narrow peaks (FWHM around 11–16 nm) associated with the resonant cavity modes appear within the enhanced broad SSE spectrum. The cavity-mode related emission peaks almost span the whole SSE spectral range (500–700 nm) though the peaks have a relatively low Q-factor (40–50) because of the imperfection of the Ag/PMMA-QDs/Ag cavity structure made by spin coating. With this simple microcavity structure, the narrow PL spectra centered in the plasmon-enhanced SSE range can be easily customized.

The microcavity structure is used for further investigation of the QDs dynamics related to the plasmon-enhanced SSE. The measured decay time of the luminescence can be expressed in terms of the radiative rate and non-radiative rate as given in Equation S4 (Supporting Information). **Figure 5e** shows that the lifetime of the SSE at 624 nm in the cavity (75.2 ns) is much shorter than that on Ag (103.6 ns). The decreased lifetime in the cavity is consistent with previously reported results of emitters in other types of cavities.^[44–47]

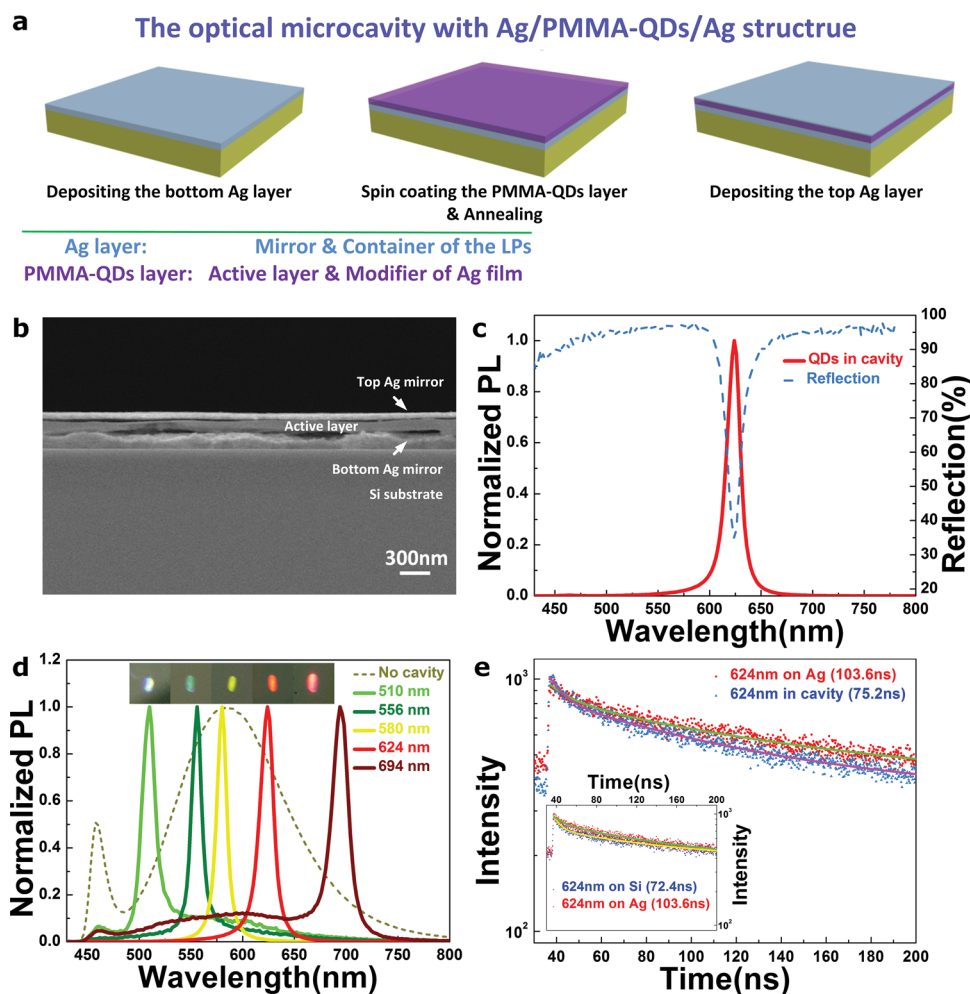


Figure 5. The plasmon-enhanced SSE in the microcavity. a) Schematic diagram of the preparation of the simple Ag/PMMA-QDs/Ag optical microcavity structure. b) The SEM image of the cross section of the microcavity. c) The PL and reflection spectra of the microcavity structure with the cavity mode at 624 nm. d) The PL spectra of the microcavities with varied active-layer thicknesses and the PMMA-CdS QDs/Ag (dashed line for reference) excited by a 405-nm laser line and detected at 0°. The inset shows the color photos of the spots on the surface of the top Ag layer excited by a 405-nm laser line. e) Comparison of the time-resolved PL (TRPL) for the microcavity and the PMMA-CdS QDs/Ag (Inset: The TRPL of PMMA-CdS QDs/Si and PMMA-CdS QDs/Ag).

The coupling between the QDs and the optical microcavity enhances the radiative decay rate k_r of the excitons in the QDs (Purcell effect). On the contrary, the plasmon-enhanced SSE results in an increasing lifetime (103.6 ns) compared to that of PMMA-QDs/Si (72.4 ns), which is related to the suppression of the non-radiative decay rate k_{nr} of the SSE by LP-coupling.

3.2. An Electroluminescence Device with Enhanced SSE

As a noble metal, Ag is a good electrode material because of its high electric conductivity, relatively low work function (ca. 4.3 eV), and good chemical stability. Here, an Ag film is used as the cathode and to form QDs/Ag couplers in the QD light-emitting diodes (QD LEDs). The QD LED consists of ITO/PEDOT:PSS/CBP:QDs/Ag (Figure 6a) (where PEDOT:PSS = poly(3,4-ethylenedioxythiophene):poly(styrene sulfonate), a hole-injection layer (HIL)). The energy-level diagram of the device is shown in Figure 6b. The semi CdZnS/ZnS core-shell QDs (470 nm) in toluene were mixed

with 4,4',N,N'-diphenylcarbazole (CBP) in chloroform and the mixture was spin coated on the PEDOT:PSS layer to form the CBP:QDs active layer. The Ag electrode (ca. 100 nm) was thermally evaporated on the CBP:QDs layer. Holes were injected from the ITO layer through the PEDOT:PSS layer whereas electrons were injected from the Ag cathode. The emission was measured at the ITO side.

The electroluminescence (EL) spectra at different bias for the QD-LED are shown in Figure 6c. The PL of the CBP:QDs is plotted for comparison. The current densities and ratios of SSE to BEE versus bias voltage are shown in Figure 6d. The BEEs of the EL spectra have larger line widths (FWHM of 24–40 nm) than that of the PL spectra (ca. 20 nm) whereas the BEEs of the EL spectra display a red-shift by about 15 nm in comparison to that of the PL spectra. The red-shift and spectral broadening may originate from the Förster energy transfer and the Joule heat in the device. When the bias is 6 V, the EL is very weak. The EL at 8 V is about 10-fold that at 6 V, whereas the intensities of the SSE are not prominent. When the bias increases to 10 V, however,

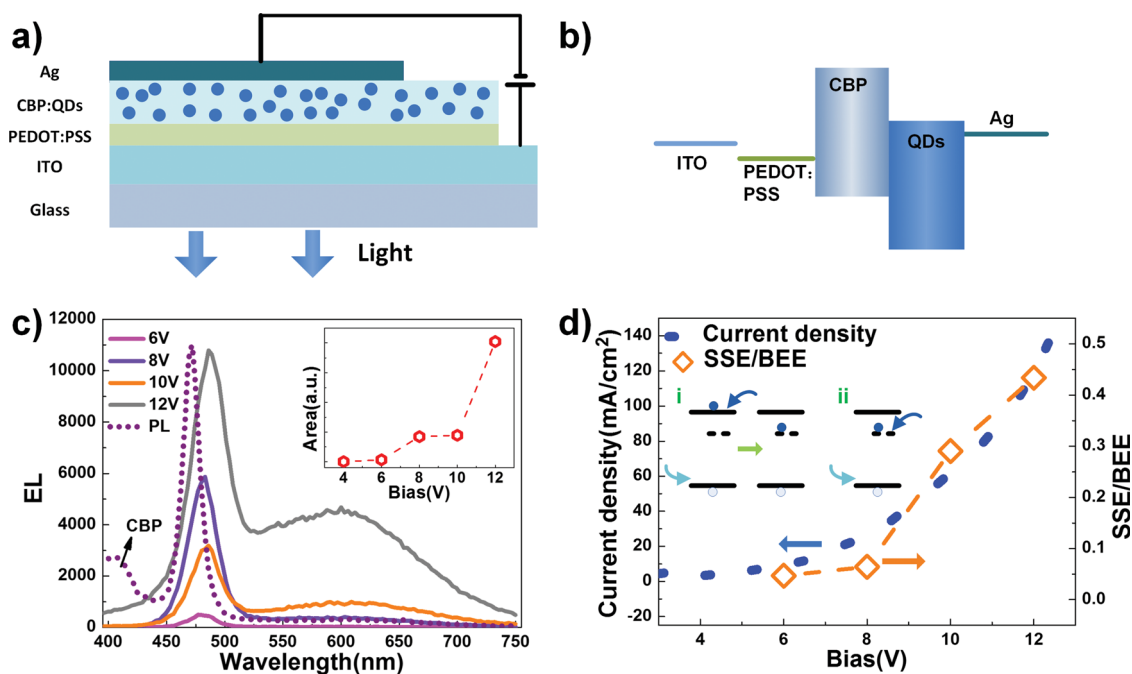


Figure 6. a) Structure diagram of device ITO/PEDOT:PSS/CBP:QDs/Ag. b) The energy-level diagram of the device. c) EL spectra of the QLED at various voltages. Inset: the area (integrated intensity) of EL spectra versus the bias. d) Current density and the ratio of SSE to BEE versus the bias of the QLED. Inset: two mechanisms for the generation of SSE excitons.

the BEE decreases while the SSE clearly increases. The ratio of SSE to BEE further increases to about 0.45 at 12 V.

The SSE difference between the EL and PL can be explained by different excitonic generation and recombination mechanisms. The SS excitons in the EL are possibly formed via the direct trapping of the injected carriers on the SSs of the QDs whereas the excitons in the PL are mainly created inside the QDs. During measurement of a PL spectrum electron–hole pairs are mainly generated inside the QDs by absorption of excitation photons. Most photon-generated carriers directly recombine inside the QD cores and, consequently, the BEE dominates the PL spectrum shown in Figure 6c. In the meantime, a fraction of the carriers may diffuse to the QD surface and be trapped by the SSs, which eventually decay by either radiative recombination (SSE) or non-radiative recombination. On the contrary, for the EL spectra shown in Figure 6c, where SSE varies with the bias voltage, the mechanisms could be quite different. In the QD LED the QDs are dispersed in the CBP host material. When the bias is small the injected electrons and holes from the two electrodes may first form excitons in the CBP, after which these excitons diffuse into the QDs by energy transfer (shown in the inset of Figure 6d). Thus the EL at smaller currents shows a relatively weak SSE. As the bias increases, both the energy and density of the injected carriers in the CBP layer increase, whereas the hot carriers may directly collide with the QDs surface and a considerable part of the injected hot electrons and holes are possibly trapped by the SSs and converted to SS excitons. We further found that this bias-sensitive SSE can also be tuned by surface-state engineering. The surface-passivated QDs show that the ratio of SSE to BEE is not sensitive to the bias voltage (Figure S8, Supporting Information).

4. Conclusions

We have demonstrated that QDs emitters can be deliberately manipulated via a combination of surface-state engineering and band-tailoring engineering. We have explored multiple functions for Ag in tuning the luminescence by forming QDs/Ag couplers, including its LP coupling, optical reflection, and electrical conduction. The chemical interaction between CdZnS QDs and Ag modifies the plasmonic properties of the couplers, which in turn influences the coupling between the SSs of the QDs emitters and LPs in Ag nanostructures, thus, the emission of the QDs is readily tuned. The SS–LP coupling can be precisely modulated by changing the SSs of the QDs by either a semi-shell capping on the QDs during synthesis or by UV irradiation after synthesis. The enhancement of the relative intensity ratio of SSE to BEE by LP coupling is over 100 whereas UV irradiation is able to shrink the intensity ratio of SSE to BEE by five times. By combining the alloyed core–shell QDs and UV irradiation, we were able to individually adjust the energy position and density of the SSs for customizable luminescence colors using single-size QDs. To illustrate the applications of the QDs/Ag plasmon couplers, we have realized multiple-function concurrence of Ag in our couplers, namely, Ag acts as LP support, reflecting mirror, and electrode. Optical microcavities with QDs sandwiched between the top and bottom Ag mirrors have been designed and fabricated in which the SSE was greatly enhanced by LPs and strongly modified by the microcavities. In the newly realized QD LEDs incorporated with a QDs/Ag plasmon coupler and simultaneously having Ag act as the cathode, the intensity ratio of SSE to BEE shows a distinct tunability through changing the bias voltage and, consequently, the EL color of the QDs is tunable as well. The new QDs/Ag plasmon

coupler opens exciting possibilities in developing novel light sources and biomarker detectors.

5. Experimental Section

Chemicals: Cadmium oxide (CdO, 99.95%), selenium powder (Se, 99.999%), oleic acid (OA, 90%), 1-octadecane (ODE, 90%), tri-*n*-octyl phosphine (TOP, 90%), and polymethylmethacrylate (PMMA, average MW 350000) powders were purchased from Alfa Aesar. Sulfur powder (99.99%), tributylphosphine (TBP, 95%), and zinc acetate dehydrate (Zn(OAc)₂·2H₂O, 99.99%) were purchased from aladdin-reagent. The PEDOT:PSS (1.3 wt% dispersion in H₂O, conductive grade) was purchased from Aldrich.

Synthesis of the CdS QDs: Typically, for CdS QDs with an emission peak at 472 nm, 2 mmol CdO powder, 3 mL OA, and 30 mL ODE were loaded in a 50 mL three-necked flask. Then the mixture was heated to 300 °C under argon atmosphere until a transparent Cd precursor was formed. The heat was then removed and 1 mL TBPS solution (S powder dissolved in TBP with 3m concentration) was swiftly injected into the flask, after which the flask was cooled naturally. The CdS QDs were centrifuged with ethanol and then re-dispersed in toluene. The wavelength of the QDs can be tuned by mainly varying the injection temperature and the reaction time.

Synthesis of the CdZnS/ZnS Core-Shell QDs and the quasi CdZnS/ZnS Core-Shell QDs: For the CdZnS/ZnS core-shell QDs, 1.5 mmol CdO, 12 mmol Zn(OAc)₂·2H₂O, 8 mL OA, and 17 mL ODE were heated at 300 °C under argon atmosphere until the transparent Cd/Zn precursor was formed. Then 3 mmol S dissolved in 6 mL ODE was swiftly injected. The mixture in the flask was heated at 300 °C for 8 min. During this time, three batches were extracted at 1, 4, and 8 min. Then, 4 mL TBPS with 3m concentration was injected for ZnS shell formation. The growth time of the shells was 30 min. After cooling, the CdZnS/ZnS QDs were centrifuged with ethanol and then re-dispersed in toluene. For the semi CdZnS/ZnS core-shell QDs, the synthesis method was similar to that stated above. The Cd, Zn element amounts were 2 mmol and 3 mmol, respectively. And the S (dissolved in ODE) for the first injection was 3 mmol, the TBPS for the second injection was 1.2 mL.

Preparation and Characterization of the Samples with SSE-IP Coupling: Half of a clean Si wafer was coated with a 60-nm Ag film by thermal evaporation. The QDs/toluene solution was then spin-coated on the Ag/Si substrate. Each wafer was cleaved into two pieces along the direction perpendicular to the boundary between the areas with Ag and without Ag. One cleaved piece was kept as a reference sample whereas the other was annealed in air at 150 °C in an oven for 30 min. The PL spectra of both the areas with and without Ag were measured.

Steady-state PL and lifetime measurements were performed using an Edinburgh FLS920 system with an excitation line of 325 nm from a Xenon lamp (for PL) and with a 405-nm picosecond laser for the lifetime experiments. The absorption measurements were performed using a UV-3600 UV-vis-NIR spectrophotometer.

Preparation of the QDLEDs: The hole-injection layer of PEDOT:PSS was spin coated onto the cleaned surface of ITO glass. The PEDOT:PSS layer was heated at 150 °C for 30 min to remove the water. A 1.5 mL solution of CBP dissolved in chloroform (50 mg mL⁻¹) was added to about 4.5 mL of a CdZnS/ZnS QDs (470 nm) dispersion in toluene (34 mg mL⁻¹). The CBP:QDs

mixture was then spin coated onto the PEDOT:PSS layer and this layer was dried by a blower to remove the residual solvent. Finally the Ag cathode (ca. 100 nm) was deposited on the CBP:QDs layer by thermal evaporation through a mask.

Supporting Information

Supporting Information is available from the Wiley Online Library or from the author.

Acknowledgements

This work was supported by the National Key Basic Research Program of China (No. 2011CB925603) and the Natural Science Foundation of China (Nos. 61290305 and 11374259).

- [1] L. E. Brus, *J. Chem. Phys.* **1984**, *80*, 4403.
- [2] W. K. Leutwyler, S. L. Bürgi, H. Burgli, *Science* **1996**, *271*, 933.
- [3] D. Norris, M. Bawendi, *Phys. Rev. B* **1996**, *53*, 16 338.
- [4] C. Kagan, C. Murray, M. Nirmal, M. Bawendi, *Phys. Rev. Lett.* **1996**, *76*, 1517.
- [5] W. W. Yu, L. Qu, W. Guo, X. Peng, *Chem. Mater.* **2003**, *15*, 2854.
- [6] D. H. Son, S. M. Hughes, Y. Yin, A. Paul Alivisatos, *Science* **2004**, *306*, 1009.
- [7] M. J. Bowers, J. R. McBride, S. J. Rosenthal, *J. Am. Chem. Soc.* **2005**, *127*, 15 378.
- [8] S. Rakshit, S. Vasudevan, *J. Phys. Chem. C* **2008**, *112*, 4531.
- [9] N. Sedat, M. Evren, A. Ozgun, P. Nihan Kosku, D. Hilmi Volkan, L. Lydia, S. Sameer, G. Nikolai, E. Alexander, *New J. Phys.* **2008**, *10*, 023 026.
- [10] K. Yu, *Adv. Mater.* **2012**, *24*, 1123.
- [11] D. A. Wheeler, J. Z. Zhang, *Adv. Mater.* **2013**, *25*, 2878.
- [12] M. A. Hines, P. Guyot-Sionnest, *J. Phys. Chem.* **1996**, *100*, 468.
- [13] L. Hu, H. Wu, C. Cai, T. Xu, B. Zhang, S. Jin, Z. Wan, X. Wei, *J. Phys. Chem. C* **2012**, *116*, 11 283.
- [14] M. J. Bowers, J. R. McBride, S. J. Rosenthal, *J. Am. Chem. Soc.* **2005**, *127*, 15 378.
- [15] D. R. Baker, P. V. Kamat, *Langmuir* **2010**, *26*, 11 272.
- [16] A. D. Dukes, P. C. Samson, J. D. Keene, L. M. Davis, J. P. Wikswo, S. J. Rosenthal, *J. Phys. Chem. A* **2011**, *115*, 4076.
- [17] T. E. Rosson, S. M. Claiborne, J. R. McBride, B. S. Stratton, S. J. Rosenthal, *J. Am. Chem. Soc.* **2012**, *134*, 8006.
- [18] S. Nizamoglu, E. Mutlugun, O. Akyuz, N. Kosku Perkgoz, H. V. Demir, L. Liebscher, S. Sapra, N. Gaponik, A. Eychmüller, *New J. Phys.* **2008**, *10*, 023 026.
- [19] J. Park, K. H. Lee, J. F. Galloway, P. C. Searson, *J. Phys. Chem. C* **2008**, *112*, 17 849.
- [20] H. H.-Y. Wei, C. M. Evans, B. D. Swartz, A. J. Neukirch, J. Young, O. V. Prezhdo, T. D. Krauss, *Nano Lett.* **2012**, *12*, 4465.
- [21] M. Tamborra, M. Striccoli, R. Comparelli, M. L. Curri, A. Petrella, A. Agostiano, *Nanotechnology* **2004**, *15*, S240.
- [22] D. F. Underwood, T. Kippeny, S. J. Rosenthal, *J. Phys. Chem. B* **2001**, *105*, 436.
- [23] C. R. Bullen, P. Mulvaney, *Nano Lett.* **2004**, *4*, 2303.
- [24] L. Hu, H. Wu, L. Du, H. Ge, X. Chen, N. Dai, *Nanotechnology* **2011**, *22*, 125 202.
- [25] S. Lin, M. M.-K. Wong, P.-K. Pat, C.-Y. Wong, S.-K. Chiu, E. Y.-B. Pun, *J. Phys. Chem. C* **2011**, *115*, 21 604.
- [26] C.-A. Lin, D.-S. Tsai, C.-Y. Chen, J.-H. He, *Nanoscale* **2011**, *3*, 1195.

- [27] T. Ozel, I. M. Soganci, S. Nizamoglu, I. O. Huyal, E. Mutlugun, S. Sapra, N. Gaponik, A. Eychmüller, H. V. Demir, *New J. Phys.* **2008**, *10*, 083 035.
- [28] F. Zhou, Z.-Y. Li, Y. Liu, Y. Xia, *J. Phys. Chem. C* **2008**, *112*, 20 233.
- [29] Q. Zhang, W. Li, C. Moran, J. Zeng, J. Chen, L.-P. Wen, Y. Xia, *J. Am. Chem. Soc.* **2010**, *132*, 11 372.
- [30] M. Drndić, M. V. Jarosz, N. Y. Morgan, M. A. Kastner, M. G. Bawendi, *J. Appl. Phys.* **2002**, *92*, 7498.
- [31] P. P. Pompa, L. Martiradonna, A. D. Torre, F. D. Sala, L. Manna, M. De Vittorio, F. Calabi, R. Cingolani, R. Rinaldi, *Nat. Nanotechnol.* **2006**, *1*, 126.
- [32] H. Yuan, S. Khatua, P. Zijlstra, M. Yorulmaz, M. Orrit, *Angew. Chem. Int. Ed.* **2013**, *52*, 1217.
- [33] K. Leong, Y. Chen, D. J. Masiello, M. T. Zin, M. Hnilova, H. Ma, C. Tamerler, M. Sarikaya, D. S. Ginger, A. K. Y. Jen, *Adv. Funct. Mater.* **2010**, *20*, 2675.
- [34] X. Cui, K. Tawa, H. Hori, J. Nishii, *Adv. Funct. Mater.* **2010**, *20*, 546.
- [35] J. Yoo, X. Ma, W. Tang, G.-C. Yi, *Nano Lett.* **2013**, *13*, 2134.
- [36] C.-H. Lu, C.-C. Lan, Y.-L. Lai, Y.-L. Li, C.-P. Liu, *Adv. Funct. Mater.* **2011**, *21*, 4719.
- [37] W. K. Bae, M. K. Nam, K. Char, S. Lee, *Chem. Mater.* **2008**, *20*, 5307.
- [38] X. Peng, *Acc. Chem. Res.* **2010**, *43*, 1387.
- [39] M. D. Regulacio, M.-Y. Han, *Acc. Chem. Res.* **2010**, *43*, 621.
- [40] R. E. Bailey, S. Nie, *J. Am. Chem. Soc.* **2003**, *125*, 7100.
- [41] J. E. B. Katari, V. L. Colvin, A. P. Alivisatos, *J. Phys. Chem.* **1994**, *98*, 4109.
- [42] D. A. Hines, M. A. Becker, P. V. Kamat, *J. Phys. Chem. C* **2012**, *116*, 13 452.
- [43] S. Keiichi, K. Satoshi, H. Shinya, C. Taeko, U.-S. Keiko, T. Tsukasa, T. Yasuhiro, K. Susumu, *Nanotechnology* **2007**, *18*, 465 702.
- [44] J. Jasieniak, C. Sada, A. Chiasera, M. Ferrari, A. Martucci, P. Mulvaney, *Adv. Funct. Mater.* **2008**, *18*, 3772.
- [45] K. J. Russell, T.-L. Liu, S. Cui, E. L. Hu, *Nat. Photonics* **2012**, *6*, 459.
- [46] A. Belarouci, F. Menchini, H. Rigneault, B. Jacquier, R. M. Montereali, F. Somma, P. Moretti, *Opt. Commun.* **2001**, *189*, 281.
- [47] N. Valappil, M. Luberto, V. M. Menon, I. Zeylikovich, T. K. Gayen, J. Franco, B. B. Das, R. R. Alfano, *Photonics Nanostruct.* **2007**, *5*, 184.

Received: January 13, 2014
Revised: February 21, 2014
Published online: April 7, 2014